Article

Canonical sound fields in the frequency-domain theory of supersonic leading-edge noise

Powles, Christopher and Chapman, C.J.

Powles, Christopher ORCID: 0000-0001-9175-2328 and Chapman, C.J. (2019) Canonical sound fields in the frequency-domain theory of supersonic leading-edge noise. Wave Motion, 86 . pp. 125-136. ISSN 0165-2125

Canonical sound fields in the frequency-domain theory of supersonic leading-edge noise

C. J. Powles[a], C. J. Chapman[b,*]

[a]*School of Physical Sciences and Computing, University of Central Lancashire, Preston, Lancashire PR1 2HE, UK*
[b]*Department of Mathematics, University of Keele, Staffordshire ST5 5BG, UK*

Abstract

This paper determines the three-dimensional structure of certain single-frequency canonical sound fields occurring in the theory of blade-vortex interaction when the flow velocity relative to the blade is supersonic. A relative velocity of this magnitude occurs at the outer part of the fan blades in an aeroengine, at which the incoming vorticity has either been ingested from the atmosphere or created in the aeroengine itself. The sound fields analysed are those produced by the leading edge of a flat-plate blade at zero angle of attack on being struck by a gust which is either (i) localised along the span, or (ii) non-localised but discontinuous. The canonical gusts of type (i) have either a delta-function or Gaussian shape, and those of type (ii) are either anti-symmetric or described by a Heaviside function; these gusts give rise to the four basic canonical sound fields. The paper also analyses a fifth sound field, produced by a single-frequency top-hat gust. This sound field has a complex structure involving aspects of both (i) and (ii), but can nevertheless be analysed in terms of the canonical sound fields. The main results of the paper are exact and approximate analytical formulae giving the dependence of the acoustic field on gust-shape and flow parameters, and also a simple formula which is ideal for numerical work. The last of these is used to assess in detail the numerical accuracy of all the approximate formulae, which are of either Fresnel or Keller type. A key result is that Keller-type formulae, representing sound rays produced in accord with the geometrical theory of diffraction, have a very wide range of validity. A companion paper (Chapman & Powles 2019) in this special issue of Wave Motion determines the canonical sound fields in the corresponding time-domain theory.

Keywords:
acoustics, blade, fan, gust, leading edge, supersonic

1. Introduction

What is the full three-dimensional structure of the sound field produced by a gust of arbitrary shape striking the leading edge of a supersonic aerofoil or fan blade? In its general form, this is a problem of some complexity, especially when account is taken of such important matters as the blade angle of attack, thickness, and camber. Substantial progress has been made over many years in related subsonic problems, of which representative work in two dimensions is [1–2] and in three dimensions is [3–8]. For the supersonic problem, the amount of published work is smaller, but important two-dimensional fields have been determined in [9–11], and three-dimensional fields in [12–17]. In the PhD thesis [18], a general analytical formula was derived for the sound field produced by a gust of arbitrary shape striking the supersonic leading edge of a flat-plate aerofoil at zero angle of attack, and it was used to calculate many two- and three-dimensional sound fields. The general formula and its derivation are in [19], and the calculated two-dimensional sound fields are in [10]. Most of the three-dimensional sound fields calculated in the thesis remain unpublished.

*Corresponding author
Email addresses: cpowles@uclan.ac.uk (C. J. Powles), c.j.chapman@keele.ac.uk (C. J. Chapman)

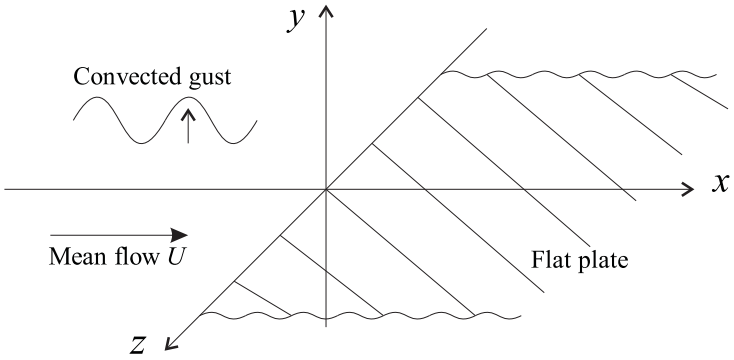

Figure 1: Gust convected at speed U in the x-direction past a stationary flat-plate aerofoil. The aerofoil occupies the half-plane $y = 0, x \geq 0$, and the leading edge lies along the z-axis.

The aim of this and the companion paper [20] is to give the most important three-dimensional canonical sound fields for the supersonic problem, making use as appropriate of [18]. One theme is the relevance of Keller's geometrical theory of diffraction in regions of space where the sound field admits a ray theory description; indeed, many of the results in this paper amount to the determination of canonical diffraction coefficients for the rays produced at an edge by a supersonically convected gust. The canonical fields provide a starting-point for the solution of more general problems by superposition and integration, and aspects of them are implicit in [12–17]. The present paper deals with single-frequency gusts (producing sound fields which are also single-frequency), whereas the companion paper concerns time-domain fields, with emphasis on impulsive pressure fields. The two papers together give a rather thorough account of the core mathematical results; for an orientation of the theory towards aeroengines, see [21].

The structure of the paper is as follows. In §2 the supersonic gust problem is formulated mathematically, and in §3 the key equations are used to determine the sound field produced by two types of localised gust, those of delta-function and of Gaussian shape. Throughout the paper, the shape of a gust refers to its spanwise shape, since in the streamwise direction the gust is sinusoidal. In §4 the effect of a discontinuity in the shape of a gust is determined, for which purpose it is convenient to distinguish anti-symmetric and Heaviside-function discontinuities. In §5 the top-hat gust is analysed; it produces an acoustic field with several distinct regions, all of which can be described using the previously found canonical expressions. Conclusions are presented in §6.

2. General theory

A flat-plate aerofoil of infinite span is assumed to occupy the half-plane $y = 0$, $x > 0$ in a coordinate system (x, y, z) in which the downstream direction is x, the vertical direction is y, and the span direction is z. The aerofoil lies in an inviscid uniform mean flow at speed U in the positive x direction, as shown in Figure 1, so that any gust convected towards it is chopped at the z-axis, i.e. at the aerofoil leading edge. This chopping action generates sound; and indeed the mathematical analysis reveals explicitly that the leading edge is the source of all the sound generated by the gust. The Mach number of the flow is $M = U/c_0$, where c_0 is the speed of sound in the fluid. A supersonic mean flow is assumed, i.e. $M > 1$. In order to account concisely for the Doppler factors which occur in the various formulae, it is convenient to use Doppler-adjusted coordinates

$$\bar{x} = x/(M^2 - 1), \quad \bar{y} = y/(M^2 - 1)^{1/2}, \quad \bar{z} = z/(M^2 - 1)^{1/2}. \tag{1}$$

The term 'Doppler-adjusted' will often be left implicit; for example, the quantities $k\bar{a}$ and $k\bar{a}^2$ introduced later will be called simply the Helmholtz number and the Rayleigh distance.

The basic datum of the problem is the upwash function $f(t - x/U, z)$, representing convection of the function $f(t, z)$ at speed U in the positive x-direction. Here t denotes time. The upwash is the vertical component of the gust velocity in the plane of the aerofoil; its Fourier transform at the leading edge $x = 0$ is

$$F(\omega, m) = \int_{-\infty}^{\infty} \int_{-\infty}^{\infty} f(t, z) \mathrm{e}^{\mathrm{i}(\omega t - mz)} \mathrm{d}t \, \mathrm{d}z, \tag{2}$$

where ω is the frequency and m is the spanwise wavenumber. The acoustic pressure $p(x, y, z, t)$ due to the gust is

$$p(x,y,z,t) = \frac{-\rho_0 M c_0 \mathrm{sgn}(y)}{(2\pi)^2 (M^2-1)^{1/2}} \int_{-\infty}^{\infty}\int_{-\infty}^{\infty} F(\omega,m) \mathrm{e}^{-\mathrm{i}\omega(t-M\bar{x}/c_0)} \mathrm{e}^{\mathrm{i}mz} J_0\left(\left\{\omega^2/c_0^2 + m^2(M^2-1)\right\}^{1/2} \bar{r}_h\right) \mathrm{d}m\, \mathrm{d}\omega, \tag{3}$$

where J_0 is the Bessel function of order zero, $\bar{r}_h = (\bar{x}^2 - \bar{y}^2)^{1/2}$ is a cylindrical coordinate measuring hyperbolic distance from the leading edge, and the integration contour in ω passes above any singularities in the integrand, to satisfy causality. Eqn. (3) applies in the Mach wedge $|\bar{y}| \le \bar{x}$ emanating downstream from the leading edge of the aerofoil; outside of this wedge there is no sound. Reference [19] provides a full derivation of (3) from the convected wave equation and boundary conditions of the problem, and also derives a far-field approximation in the form $p \simeq p_+ + p_-$ where

$$p_\pm(x,y,z,t) = \frac{-\rho_0 M c_0 \mathrm{sgn}(y)}{(2\pi)^2 (M^2-1)} \frac{1}{\bar{R}_h} \int_{-\infty}^{\infty} F(\omega, \pm\frac{\omega}{c_0}(M^2-1)^{-1/2} \tan\bar{\theta}_h) \mathrm{e}^{-\mathrm{i}\omega(t-M\bar{x}/c_0 \mp \bar{R}_h/c_0)} \mathrm{d}\omega. \tag{4}$$

Here $\bar{R}_h = (\bar{x}^2 - \bar{y}^2 - \bar{z}^2)^{1/2}$ is a hyperbolic polar distance from the origin, and $\bar{\theta}_h$ is a hyperbolic angle relative to the vertical plane $z = 0$, defined so that $\tan\bar{\theta}_h = -\bar{z}/\bar{R}_h$. Eqn. (4) assumes that the upwash is of bounded spanwise extent about the origin and that the Fourier transform $F(\omega, m)$ has no singularities in the complex m plane; it applies in the Mach cone $|\bar{y}^2 + \bar{z}^2|^{1/2} \le \bar{x}$, outside of which there is no far field, given the localised upwash. All Mach wedges and cones extend downstream of points on the leading edge, with width increasing downstream. The quantities $\bar{r}_h$ and $\bar{R}_h$ are always real; terms containing them in formulae should be put equal to zero at positions which would make them imaginary, i.e. outside of the corresponding wedge or cone. Eqns. (3) and (4) are the fundamental equations of supersonic leading edge noise for a flat-plate aerofoil at zero angle of attack.

3. Localised gusts

3.1. The delta-function gust

A delta-function gust in the vertical plane through the origin is specified by the upwash function

$$f(t - x/U, z) = v_0 \mathrm{e}^{-\mathrm{i}\omega_0(t-x/U)} \delta(z/a). \tag{5}$$

Its Fourier transform at the leading edge $x = 0$, as given by (2), is

$$F(\omega, m) = 2\pi v_0 a \delta(\omega - \omega_0). \tag{6}$$

Here v_0 is a vertical component of velocity, and a is a reference length; the gust strength is the integral over the leading edge of the term $v_0\delta(z/a)$ in (5), i.e. $v_0 a$, and this strength appears with a factor 2π in (6).

Insertion of (6) into the pressure integral (3), followed by integration with respect to ω, leaves a Bessel-function integral of standard type. Evaluation of this integral yields the pressure field in the explicit form

$$p(x,y,z,t) = \frac{-\rho_0 M c_0 \bar{v}_0 \mathrm{sgn}(y)}{\pi} \frac{\bar{a}}{\bar{R}_h} e^{-i\omega_0(t-M\bar{x}/c_0)} \cos(k\bar{R}_h), \tag{7}$$

where $k = \omega_0/c_0$ is the free-space wavenumber. The bars on $\bar{v}_0$ and $\bar{a}$ indicate that Doppler factors have been applied according to the rule implicit in (1), that streamwise quantities are to be divided by $M^2 - 1$, and transverse quantities (vertical and spanwise) are to be divided by $(M^2-1)^{1/2}$. Thus $\bar{v}_0 = v_0/(M^2-1)^{1/2}$ and $\bar{a} = a/(M^2-1)^{1/2}$. This convention is adopted throughout the paper. Expression (7) may also be written in terms of the the spherical Bessel function y_0, or the Bessel function $Y_{1/2}$, by means of the relations

$$\mathrm{y}_0(s) = \left(\frac{\pi}{2s}\right)^{\frac{1}{2}} Y_{1/2}(s) = \frac{-\cos(s)}{s}. \tag{8}$$

Thus (7) is in effect a separable solution of the wave equation, of standard type, but expressed in transformed coordinates.

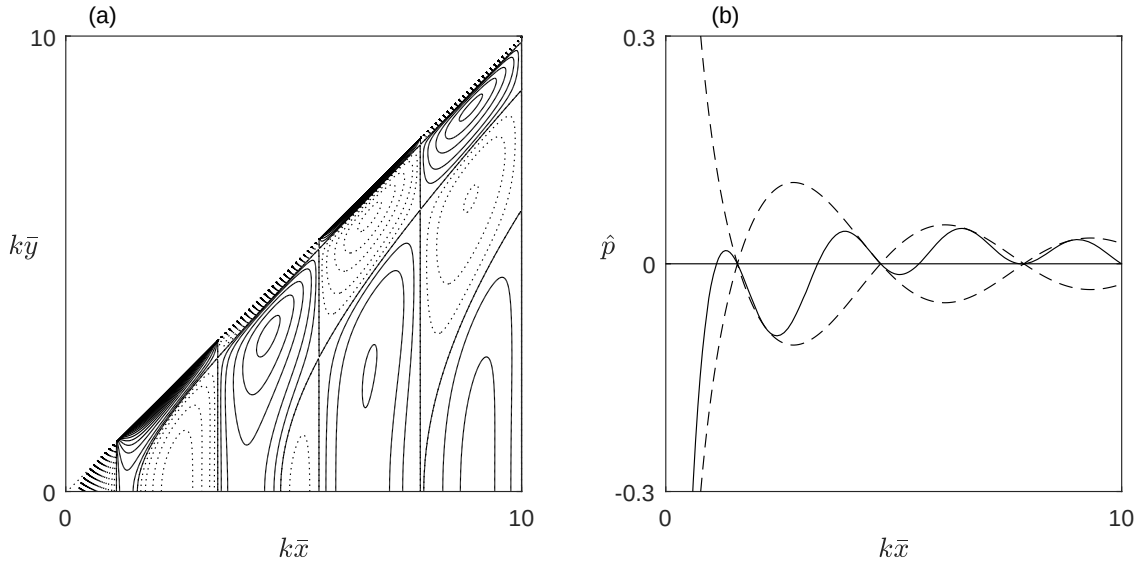

Figure 2: (a) Scaled pressure contours for the delta-function gust in the vertical plane $z = 0$ at time $t = 0$ for Mach number $M = \sqrt{2}$; axes are $k\bar{x}$ streamwise and $k\bar{y}$ vertically, where $k = \omega_0/c_0$ is the free-space wavenumber. Solid lines are contours of positive or zero pressure, and dotted lines are contours of negative pressure. Contour values are $0, \pm 0.01, \pm 0.025$, and then at intervals of ± 0.025. (b) The solid line is the scaled pressure on the $k\bar{x}$ axis in (a), and the dashed lines are its envelope $\pm(1/\pi)\cos(k\bar{R}_h)/(k\bar{R}_h)$.

Figure 2(a) is a contour plot of the real part of the pressure field (7) at time $t = 0$ for Mach number $M = \sqrt{2}$ on a vertical section through the x axis, and Figure 2(b) shows the pressure field on the axis itself, together with its envelope. The pressure has been scaled by $(\rho_0 M c_0 \bar{v}_0)(k\bar{a})$ to make it dimensionless and reduce it to similarity form in $Mk\bar{x}$ and $k\bar{R}_h$. The pressure field may be called the three-dimensional supersonic edgelet, since it is the sound produced by an individual point on the leading edge. This field is much simpler than the subsonic three-dimensional edgelet, given as a contour integral in [8], where it is referred to as the edgelet function E_1; and it is slightly simpler than the two-dimensional supersonic edgelet given in [10]. Expression (7) applies in the Mach cone $|\bar{y}^2 + \bar{z}^2|^{1/2} < \bar{x}$ emanating downstream from the origin; elsewhere the field is zero. As the surface $\bar{R}_h = 0$ of the cone is approached, the pressure field acquires an inverse square root singularity, because of the pattern of signs in the hyperbolic polar coordinate $\bar{R}_h = (\bar{x}^2 - \bar{y}^2 - \bar{z}^2)^{1/2}$. Such a singularity in pressure is acceptable, because its integral over the blade surface gives a finite force. Except for antisymmetry in y (the vertical coordinate), the field is cylindrically symmetric about the x-axis, i.e. about the stream direction.

3.1.1. Green's function

The edgelet field may be used to give a Green's function representation of the sound produced by the upwash

$$f(t - x/U, z) = v_0 \mathrm{e}^{-\mathrm{i}\omega_0(t-x/U)} g(z), \tag{9}$$

where $g(z)$ is an arbitrary function specifying the shape of the gust along the leading edge. The function $g(z)$ is dimensionless. If for the moment we denote the field (7) by $p_\mathrm{E}(x, y, z, t)$, then the pressure field due to the arbitrary

gust (9) is

$$p(x,y,z,t) = \frac{1}{\bar{a}} \int_{\bar{z}-\bar{r}_h}^{\bar{z}+\bar{r}_h} g(z_0)\, p_{\mathrm{E}}(x,y,z-z_0,t)\, \mathrm{d}\bar{z}_0. \tag{10}$$

Here the integration is over that part of the leading edge which can influence the pressure at (x,y,z). A change of variable to the angle θ defined by $\bar{z}_0 = \bar{r}_h \cos\theta + \bar{z}$, where $-\pi < \theta < 0$, gives the exact result

$$p(x,y,z,t) = \frac{-\rho_0 M c_0 \bar{v}_0 \mathrm{sgn}(y)}{\pi} \mathrm{e}^{-\mathrm{i}\omega_0(t-M\bar{x}/c_0)} \int_{-\pi}^{0} g\left((M^2-1)^{1/2}(\bar{r}_h\cos\theta+\bar{z})\right) \cos\left(k\bar{r}_h \sin\theta\right)\, \mathrm{d}\theta. \tag{11}$$

Expression (11) is free of singularities and has a finite range of integration; this makes it especially useful for numerical integration. On the Mach wedge $\bar{r}_h = 0$, it gives explicitly

$$p(x,y,z,t) = -\rho_0 M c_0 \bar{v}_0 \mathrm{sgn}(y) \mathrm{e}^{-\mathrm{i}\omega_0(t-M\bar{x}/c_0)} g(z) = \frac{-\rho_0 M c_0 \mathrm{sgn}(y)}{(M^2-1)^{1/2}} f(t-M\bar{x}/c_0, z), \tag{12}$$

a remarkable exact result for a fully three-dimensional problem. The first result of this type was obtained in [12], for a time-domain field, and its single-frequency form is derived in [19]. On the Mach wedge at a given value of z, the acoustic field is influenced only by the leading edge upwash at the same value of z; this explains the proportionality of $p(x,y,z,t)$ to $g(z)$ in (12). A striking feature of the result is the absence of attenuation with distance from the source. Thus the competing influences of (i) decay in amplitude with distance from the source, and (ii) growth in amplitude as the Mach wedge is approached, are perfectly balanced on the Mach wedge itself.

3.2. The Gaussian gust

An account of the Gaussian gust is given in [19], as an illustration of the general theory there developed. Here we extend this account to include plots and further discussion of the structure of the acoustic field. A Gaussian gust has upwash

$$f(t-x/U, z) = (2\pi)^{-1/2} v_0 \mathrm{e}^{-\mathrm{i}\omega_0(t-x/U)} \mathrm{e}^{-(z/a)^2/2}, \tag{13}$$

for which

$$F(\omega, m) = 2\pi v_0 a \delta(\omega-\omega_0) \mathrm{e}^{-(ma)^2/2}. \tag{14}$$

The strength of the gust, i.e. the spanwise integral of $(2\pi)^{-1/2} v_0 \mathrm{e}^{-(z/a)^2/2}$, is $v_0 a$. In expression (3) for the pressure, evaluation of the ω integral in is immediate, but the resulting integral in m is not tractable analytically. However, from (4) the far-field approximation $p \simeq p_+ + p_-$ is

$$p(x,y,z,t) \simeq \frac{-\rho_0 M c_0 \bar{v}_0 \mathrm{sgn}(y)}{\pi} \mathrm{e}^{-\mathrm{i}\omega_0(t-M\bar{x}/c_0)} \frac{\bar{a}}{\bar{R}_h} \cos(k\bar{R}_h)\, \mathrm{e}^{-(k\bar{a}\tan\bar{\theta}_h)^2/2}, \tag{15}$$

where $\tan\bar{\theta}_h = -\bar{z}/\bar{R}_h$. In the limit $a \to 0$ and $v_0 \to \infty$, with $v_0 a$ fixed, this must give the field due to a delta-function gust; comparison of (15) with (7) confirms that this is so.

For general a, approximation (15) loses accuracy near the two lines where the Mach cone $\bar{R}_h = 0$ touches the Mach wedge $\bar{r}_h = 0$, or equivalently where the Mach cone intersects the vertical plane $z = 0$. The reason is that the approximation (15) then tends to infinity as $\bar{R}_h \to 0$, whereas the exact expression (12), with $g(z) = (2\pi)^{-1/2}\mathrm{e}^{-(z/a)^2/2}$, shows that on these two lines the field is finite everywhere, and is in fact exactly

$$p(x,y,0,t) = \frac{-\rho_0 M c_0 \bar{v}_0 \mathrm{sgn}(y)}{(2\pi)^{1/2}} \mathrm{e}^{-\mathrm{i}\omega_0(t-M\bar{x}/c_0)}. \tag{16}$$

This field on the two lines does not attenuate with distance from the source, as noted in general after (12). Our formulae (15) and (16) differ slightly from those in [19] because of a different multiplicative factor in the definition of the upwash.

Figure 3 gives contour plots of the pressure field on vertical transverse sections $\bar{x} = k\bar{a}^2/2$ and $\bar{x} = 2k\bar{a}^2$ for Mach number $M = \sqrt{2}$ and Helmholtz number $k\bar{a} = 4$. Here we refer the streamwise coordinate $\bar{x}$ to the Rayleigh distance

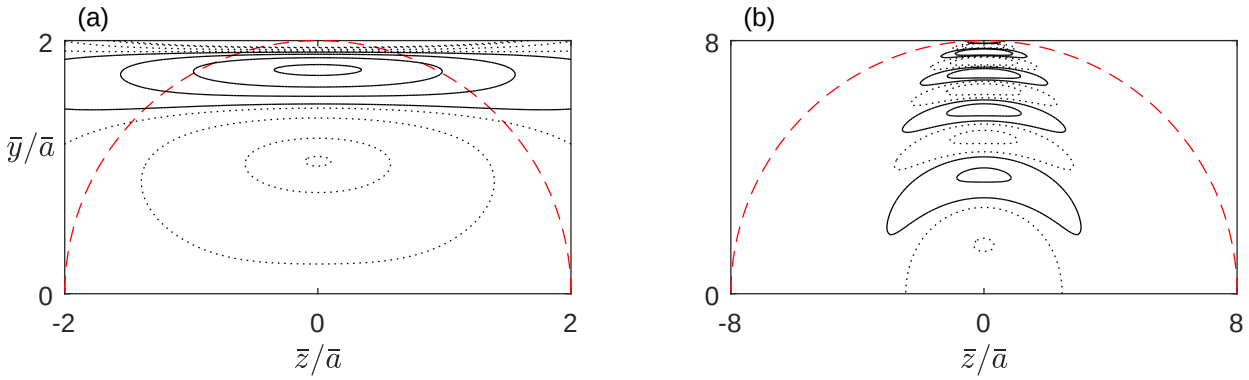

Figure 3: Scaled pressure contours for the Gaussian gust on vertical sections (a) $\bar{x} = k\bar{a}^2/2$ and (b) $\bar{x} = 2k\bar{a}^2$ for Mach number $M = \sqrt{2}$ and Helmholtz number $k\bar{a} = 4$; axes are $\bar{z}/\bar{a}$ spanwise and $\bar{y}/\bar{a}$ vertically. The free-space wavenumber is $k = \omega_0/c_0$, and the Rayleigh distance is $k\bar{a}^2$. Solid lines are contours of positive pressure, and dotted lines are contours of negative pressure. Contour values in order from a small dotted circle to a small solid circle are (a) (−.115, −.1, −.05, −.01, .01, .05, .1, .15) and (b) (−.04, −.01, .01, .04). The dashed semi-circles are sections of the Mach cone $\bar{R}_h = 0$.

$k\bar{a}^2$, because (provided $k\bar{a} > 1$) this is the distance at which far-field approximations start to apply. Thus plot 3(a) gives the near field, and plot 3(b) gives the far field. The former is obtained by accurate numerical evaluation of (11) with $g(z)$ in (9) taken to be $(2\pi)^{-1/2}\mathrm{e}^{-(z/a)^2/2}$; while for the latter, either (11) or (15) may be used, as on the scale of the plot the difference is very slight. As $\bar{x}$ increases beyond about $2k\bar{a}^2$, plots of exact and approximate formulae rapidly become indistinguishable. We scale the pressure by $\rho_0 M c_0 \bar{v}_0$, to make it dimensionless, and also omit the factor $\mathrm{e}^{-\mathrm{i}\omega_0(t-M\bar{x}/c_0)}$, which is equivalent to plotting the pressure at a particular time, namely $t = M\bar{x}/c_0$. This time is of no significance, because all fields are single-frequency. Contours of positive pressure are plotted as solid lines, and contours of negative pressure as dotted lines. The dashed circles are the intersections of the plotting planes with the Mach cone.

Figure 3(b) shows that the far field has the structure of a cylindrically symmetric wave modulated by a directivity function; the maximum amplitude is in the vertical plane $z = 0$, and the amplitude decreases rapidly as the Mach cone is approached, except at the top of the figure. This is the structure of the pressure field (15): the cylindrically symmetric wave is $\cos(k\bar{R}_h)$, and the directivity function is $\mathrm{e}^{-(k\bar{a}\tan\bar{\theta}_h)^2/2}$. Since the exponent here is proportional to $-\tan^2\bar{\theta}_h$, the field tends exponentially fast to zero as the Mach cone $\bar{R}_h = 0$ is approached (where $\bar{\theta}_h = \pm\pi/2$), notwithstanding the term $1/\bar{R}_h$ in (15). At high frequencies the field is highly directional, effectively confined to a narrow zone $\tan\bar{\theta}_h = O((k\bar{a})^{-1})$ about the vertical plane $z = 0$.

4. Spanwise discontinuous gusts

4.1. The basic anti-symmetric discontinuity

The simplest discontinuous gust has the anti-symmetric upwash function

$$f(t - x/U, z) = v_0 \mathrm{e}^{-\mathrm{i}\omega_0(t-x/U)}\,\mathrm{sgn}(z), \tag{17}$$

in which the sign function (signum) is defined by $\mathrm{sgn}(z) = \pm 1$ for $z \gtrless 0$ and $\mathrm{sgn}(0) = 0$. Its Fourier transform at the leading edge $x = 0$ is

$$F(\omega, m) = -4\pi\mathrm{i}v_0 \frac{\delta(\omega - \omega_0)}{m}. \tag{18}$$

As the gust has no length scale, the pressure field depends on frequency and position only in the combinations kx, ky, and kz, so that a change of frequency merely re-scales the pressure field, without altering its pattern.

Inside the Mach cone $\bar{R}_h = 0$, the acoustic field produced by (17) is three-dimensional; elsewhere the field is two-dimensional. It follows from a basic two-dimensional result in [10] that outside the Mach cone, but inside the

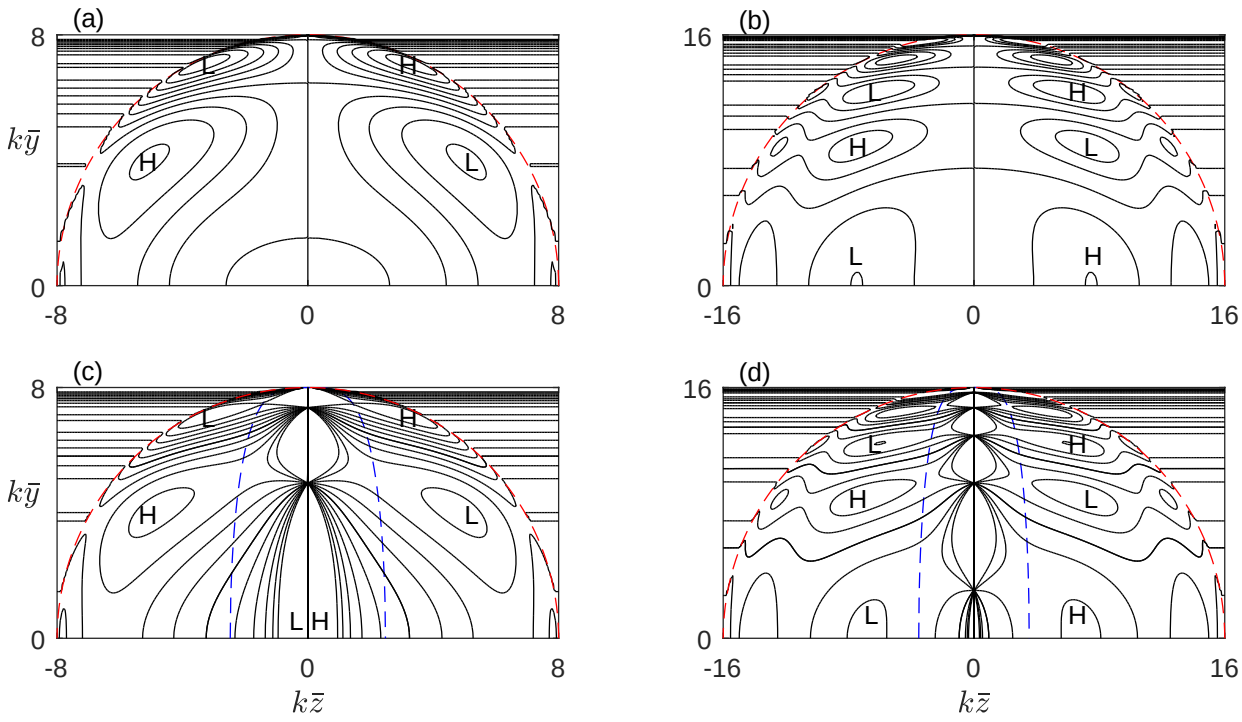

Figure 4: Scaled pressure contours on transverse vertical sections for an anti-symmetric gust convected at Mach number $M = \sqrt{2}$. (a) accurate plot on $k\bar{x} = 8$ from Eqn (11); (b) accurate plot on $k\bar{x} = 16$; (c) Keller approximation to (a), using Eqn (21) with coefficients (26); (d) Keller approximation to (b). Contour values in (a), (c) are −0.5 to 0.5, and in (b), (d) are −0.25 to 0.25, marked low (L) to high (H). The dashed semi-circles are sections of the Mach cone $\bar{R}_h = 0$, and the dashed half-ovals are sections of the surface (28) for $\sigma = 0.5$, outside of which the Keller approximation applies. In (c), (d) the Keller approximation has a singular limit $\pm\infty$ along the vertical axis $z = 0$.

Mach wedge $\bar{r}_h = 0$, the field is

$$p(x, y, t) = -\rho_0 M c_0 \bar{v}_0 \operatorname{sgn}(y) \operatorname{sgn}(z) \mathrm{e}^{-\mathrm{i}\omega_0(t - M\bar{x}/c_0)} \mathrm{J}_0(k\bar{r}_h). \tag{19}$$

Omission of the term sgn(z) from (19) gives the two-dimensional field produced by the upwash (17) with sgn(z) omitted. Thus in what follows, the new aspect is the sound field inside the Mach cone. This highly three-dimensional field is the effect of the discontinuity in the upwash, and is the transition region between fields of type (19) when z changes sign. The field may be computed numerically from the integral (11), with $g(z)$ in (9) taken to be sgn(z); the integral cannot be evaluated analytically, except as a type of incomplete Bessel function. Figures 4(a, b) are accurate contour plots of the field on vertical transverse sections $k\bar{x} = 8, 32$ for Mach number $M = \sqrt{2}$. The oscillations in pressure inside the Mach cone are evident, as is the two-dimensional nature of the field outside the cone, indicated by the straight-line contours parallel to the z axis.

4.1.1. The Fresnel approximation

The far-field approximation (4) does not apply to the discontinuous gust (17), because of the pole in the m-plane in the Fourier transform (18). Nevertheless, an accurate approximation to the field inside the Mach cone is available in terms of Fresnel integrals. This may be obtained by first evaluating the ω integral in the field representation (3), to leave an integral in the spanwise wavenumber m. Transformation to the integration variable χ defined by $m = (\omega/c_0)(M^2 - 1)^{-1/2} \sinh\chi$, followed by a steepest descent analysis involving the large-argument approximation

$$J_0(k\bar{r}_h) \simeq \left(\frac{2}{\pi}\right)^{1/2} \frac{\cos(k\bar{r}_h - \pi/4)}{(k\bar{r}_h)^{1/2}} \tag{20}$$

(and equivalently for argument $k\bar{R}_h$), reveals that a saddle point collides with a pole as the vertical plane $z = 0$ is approached. This collision requires the use of Fresnel integrals for a uniform description of the field around the plane $z = 0$, as explained in detail in [18, 22]. The principal result is the uniform approximation

$$p(x, y, z, t) \simeq \frac{-\rho_0 M c_0 \bar{v}_0 \,\mathrm{sgn}(y)}{\pi} \mathrm{e}^{-\mathrm{i}\omega_0(t - M\bar{x}/c_0)} \left\{ \alpha \frac{\sin(k\bar{R}_h)}{k\bar{R}_h} + \beta \frac{\cos(k\bar{r}_h)}{(k\bar{r}_h)^{1/2}} + \gamma \frac{\sin(k\bar{r}_h)}{(k\bar{r}_h)^{1/2}} \right\}, \tag{21}$$

where

$$\alpha = \left(\frac{2^{1/2}\, \bar{R}_h/\bar{r}_h}{(1 - \bar{R}_h/\bar{r}_h)^{1/2}} - \frac{2\bar{R}_h}{|\bar{z}|} \right) \mathrm{sgn}(z), \quad \beta = 2\pi^{\frac{1}{2}} C\left(\left(\frac{2k(\bar{r}_h - \bar{R}_h)}{\pi} \right)^{\frac{1}{2}} \right) \mathrm{sgn}(z), \quad \gamma = 2\pi^{\frac{1}{2}} S\left(\left(\frac{2k(\bar{r}_h - \bar{R}_h)}{\pi} \right)^{\frac{1}{2}} \right) \mathrm{sgn}(z), \tag{22}$$

and the Fresnel integrals (C, S) are defined by

$$C(s) = \int_0^s \cos\left(\frac{\pi\eta^2}{2} \right) \mathrm{d}\eta, \quad S(s) = \int_0^s \sin\left(\frac{\pi\eta^2}{2} \right) \mathrm{d}\eta. \tag{23}$$

The only region of space in which the Fresnel approximation (21) loses accuracy is very close to the leading edge, for $k\bar{r}_h \lesssim 1$. In Figures 4(a, b), for $k\bar{x} = 8, 32$, the approximate fields would be indistinguishable from the exact fields plotted. In order to see a difference between exact and approximate fields, it is necessary to take a section at a value of x such that $k\bar{x} \lesssim 1$.

The limit as $z \to 0$ of the Fresnel approximation (21) to the pressure is zero, notwithstanding the term in $1/|\bar{z}|$ in the coefficient α, because of cancellations. An expansion in powers of z shows that the leading-order small-z approximation is

$$p(x, y, z, t) \simeq \frac{-\rho_0 M c_0 \bar{v}_0 \mathrm{sgn}(y)}{\pi} \mathrm{e}^{-\mathrm{i}\omega_0(t - M\bar{x}/c_0)} \frac{2\bar{z}}{\bar{r}_h} \cos(k\bar{r}_h). \tag{24}$$

This has the form of a two-dimensional field multiplied by z, and is accurate near the plane $z = 0$. Eqn (24) is confirmed in Figures 4(a, b) by the contour of zero pressure along the y axis and the shape of the contours nearby.

4.1.2. The Keller approximation

At positions not too close to the vertical plane $z = 0$, a very simple approximation to the field may be obtained in accord with Keller's geometrical theory of diffraction by using the large-argument approximations

$$C(s) \simeq \frac{1}{2} + \frac{1}{\pi s} \sin\left(\frac{\pi s^2}{2} \right), \qquad S(s) \simeq \frac{1}{2} - \frac{1}{\pi s} \cos\left(\frac{\pi s^2}{2} \right) \tag{25}$$

to the Fresnel integrals in (22). It is then found in (21) that the trigonometric terms deriving from (25) cancel the first term in the coefficient α, to leave an approximation of the same form as (21), but with simpler coefficients

$$\alpha = \frac{-2\bar{R}_h}{\bar{z}}, \qquad \beta = \gamma = \pi^{1/2} \,\mathrm{sgn}(z). \tag{26}$$

Since $\beta = \gamma$, the last two terms in (21) can be grouped into the single term

$$(2\pi)^{1/2} \,\mathrm{sgn}(z) \, \frac{\cos(k\bar{r}_h - \pi/4)}{(k\bar{r}_h)^{1/2}}. \tag{27}$$

This includes the phase term $-\pi/4$ explicitly, and may be compared with (20).

The approximation obtained using the coefficients (26) is plotted in Figures 4(c, d) on transverse sections corresponding to those in Figures 4(a, b). The form of the Fresnel integrals in (22) shows that the approximation is expected to be accurate outside the region bounded by the surface $k(\bar{r}_h - \bar{R}_h) = \pi\sigma^2/2$, where σ is an order-one constant, i.e.

$$k\bar{r}_h = \frac{(k\bar{z})^2}{\pi\sigma^2} + \frac{\pi\sigma^2}{4} \tag{28}$$

after rearranging and squaring. This equation is quadratic in $(k\bar{r}_h, k\bar{z})$ but quartic in $(k\bar{x}, k\bar{y}, k\bar{z})$; it reduces to a parabola in the horizontal plane $y = 0$, but is an oval-shaped quartic in vertical planes at fixed x. In these planes, the oval curve intersects the y and z axes where

$$k\bar{y} = \pm\left\{(k\bar{x})^2 - \left(\frac{\pi\sigma^2}{4}\right)^2\right\}^{1/2}, \quad k\bar{z} = \pm(\pi\sigma^2)^{1/2}\left(k\bar{x} - \frac{\pi\sigma^2}{4}\right)^{1/2}, \tag{29}$$

provided that $k\bar{x} > \pi\sigma^2/4$. It is found numerically that (28) with the choice $\sigma \simeq 0.5$ defines a sharp transition between the region outside the oval, where the approximation is highly accurate, and the region inside, where the approximation fails on account of its singular limit along $z = 0$. The oval curve for $\sigma = 0.5$ is shown as a dashed line in Figures 4(c, d). The figures show that the approximation based on (21), (26), and (27) applies in a very large region, and captures all of the oscillations in the pressure field.

Mathematically, points inside the oval correspond to close enough approach of a saddle point and pole in the original contour integral that their contributions interfere [22], and cannot be determined separately. Provided the saddle and pole are far enough apart, the former gives the term in $(k\bar{R}_h)^{-1}\sin(k\bar{R}_h)$, representing spherically spreading rays from the origin, and, independently, the latter gives the term in $(k\bar{r}_h)^{-1/2}\cos(k\bar{r}_h - \pi/4)$, representing cylindrically spreading rays from the leading edge. In this way approximation (21) with coefficients (26) may be understood in terms of Keller's geometrical theory of diffraction and diffracted rays. Thus the region in space where the coefficients (26) may be used is the region where the acoustic field admits a ray theory description. As we have seen, this is a large region, and our approach in effect calculates the canonical diffraction coefficients of the Keller theory.

4.2. The Heaviside discontinuity

The Heaviside gust has the upwash function

$$f(t - x/U, z) = v_0 \mathrm{e}^{-\mathrm{i}\omega_0(t-x/U)}\,\mathrm{H}(z), \tag{30}$$

in which the Heaviside function $\mathrm{H}(z)$ takes the values $(1, 0)$ for $z \gtrless 0$. The acoustic field produced by this gust is three-dimensional within the Mach cone from the origin, and two-dimensional in that part of the Mach wedge for $z > 0$ which lies outside the Mach cone. Elsewhere, there is no acoustic field, because there are no sources for negative z. The identity $\mathrm{H}(z) = (\mathrm{sgn}(z) + 1)/2$ shows that the field is the mean of the anti-symmmetric field found already and the two-dimensional field indicated after (19). Thus if these fields are denoted p_1 and p_2, then the acoustic field produced by the gust (30) is simply $p = (p_1 + p_2)/2$, so that the properties of this field, both numerical and analytical, can be obtained at once from our previous results. Of particular interest is the Fresnel transition layer across the vertical plane $z = 0$, which is of the same type as the shadow boundary layer in a diffracted field. In the plane $z = 0$, the field is $p_2/2$.

Figures 5(a, b) are accurate contour plots of the pressure field on the vertical transverse sections $k\bar{x} = 8, 32$ for Mach number $M = \sqrt{2}$. They are obtained by taking p_1 to be the anti-symmetric field found in §4.1, computed numerically from the representation (11), and p_2 to be the field (19) with the term $\mathrm{sgn}(z)$ omitted. The figure makes evident the decay in field amplitude to zero as the negative-z side of Mach cone is approached, and also the two-dimensional field shape on the positive-z side.

4.2.1. The Fresnel approximation

A uniform approximation to the acoustic field is readily obtained. Since the two-dimensional field p_2 has an approximation of the form (21) with $\alpha = 0$ and $\beta = \gamma = \pi^{1/2}$, by (20), it is sufficient to take the mean of these values of (α, β, γ) and those in (22). The result is a Fresnel approximation to the acoustic field produced by the Heaviside gust (30).

Just as for the anti-symmetric gust, the only region in which the Fresnel approximation loses accuracy is close to the leading edge, i.e. for $k\bar{r}_h \lesssim 1$. In Figures 5(a, b), for $k\bar{x} = 8, 32$, the approximate fields would be indistinguishable from the exact fields which have been plotted. The approximation is continuous and accurate across the Mach cone, and also across the vertical plane $z = 0$. In order to see a difference between exact and approximate fields, it is necessary to take a section at a value of x such that $k\bar{x} \lesssim 1$.

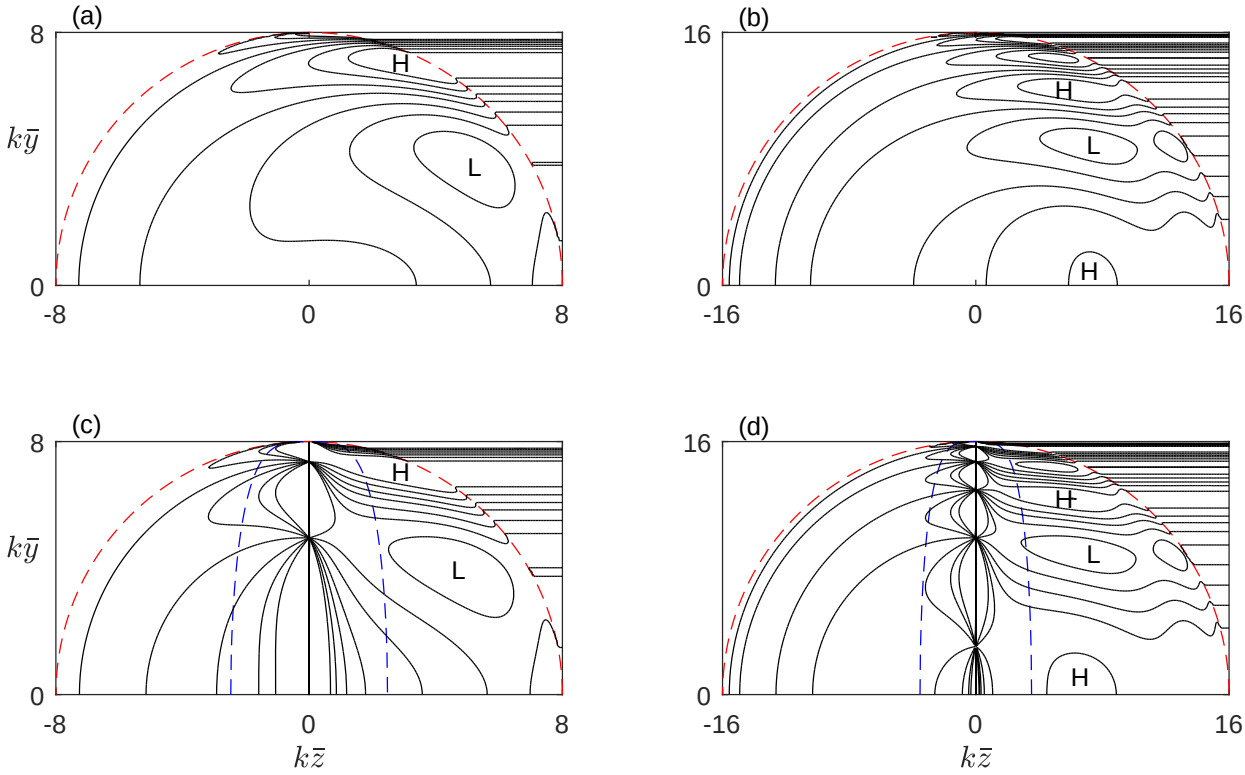

Figure 5: Scaled pressure contours on vertical sections for a Heaviside gust convected at Mach number $M = \sqrt{2}$. (a) accurate plot on $k\bar{x} = 8$; (b) accurate plot on $k\bar{x} = 16$; (c) Keller approximation to (a), using Eqn (21) with coefficients (31); (d) Keller approximation to (b). Contour values are -0.3 to 0.3, marked low (L) to high (H). The dashed semi-circles are sections of the Mach cone $\bar{R}_h = 0$, and the dashed half-ovals are sections of the surface (28) for $\sigma = 0.5$, outside of which the Keller approximation applies. In (c), (d) the Keller approximation has a singular limit $\pm\infty$ along the vertical axis $z = 0$.

4.2.2. The Keller approximation

A much simpler approximation is available at positions not too close to the vertical plane $z = 0$, because (as for the anti-symmetric gust) the Fresnel integrals in (22) may then be replaced by their large-argument forms (25). The mean of the resulting values of (α, β, γ) for p_1 and p_2 gives the Heaviside gust values

$$\alpha = \frac{-\bar{R}_h}{\bar{z}}, \qquad \beta = \gamma = \pi^{1/2}\,\mathrm{H}(z). \tag{31}$$

The last two terms in braces in (21) may then be grouped into a single term of the same form as (27), but with $\mathrm{sgn}(z)$ replaced by $\mathrm{H}(z)$. The resulting approximation obtained by using the coefficients (31) in (21) is plotted in Figures 5(c, d); the approximation is valid outside of the dashed ovals shown in the figures, which come from Eqns (28) and (29), and it has the same ray interpretation in terms of Keller's geometrical theory of diffraction. All of the previous discussion of the Keller theory applies. Thus as before, ray theory is applicable in a large region of space, and the Keller approximation captures all the oscillations in the pressure field.

5. The single-frequency top-hat gust

A top-hat gust striking the segment $-a < z < a$ of the leading edge has upwash

$$f(t - x/U, z) = v_0 \mathrm{e}^{-\mathrm{i}\omega_0(t-x/U)}\,\mathrm{H}(z/a, -1, 1), \tag{32}$$

in which the top-hat function $\mathrm{H}(s, s_0, s_1)$ takes the value 1 for $s_0 < s < s_1$ and zero elsewhere. The acoustic field produced by this gust is three-dimensional inside the Mach cones from the points $z = \pm a$ on the leading edge, and two-dimensional in that part of the Mach wedge lying between these cones. Elsewhere the field is zero, because there are no sources for $|z| > a$. The shape of the various regions may be visualised by noting that the Mach cones touch the Mach wedge along lines of intersection with planes $z = \pm a$.

The identity

$$\mathrm{H}(z/a,\, -1,\, 1) = \frac{1}{2}(\mathrm{sgn}(z + a) - \mathrm{sgn}(z - a)) \tag{33}$$

shows that the acoustic field is half the difference between two anti-symmetric fields of the type found in §4.1, after translating by $\pm a$ in the z-direction. We shall use subscripts $\pm$ to indicate that z in an expression has been replaced by $z \pm a$, so that, for example,

$$\bar{R}_{h\pm} = (\bar{x}^2 - \bar{y}^2 - (\bar{z} \pm \bar{a})^2)^{1/2}. \tag{34}$$

The fields in §4.1, with z replaced by $z \pm a$, will be denoted $p_\pm$. With this convention, p_+ is anti-symmetric about $z = -a$, and p_- is anti-symmetric about $z = a$. The acoustic field produced by the top-hat gust (32) is $p = (p_+ - p_-)/2$, which gives the properties of the field in terms of the results in previous sections. Alternatively, to avoid the cancellations which occur in $p_+ - p_-$, one can work directly with the Fourier transform of (32), which on the leading edge $x = 0$ is

$$F(\omega, m) = 4\pi v_0 \delta(\omega - \omega_0) \frac{\sin(ma)}{m}. \tag{35}$$

This has a finite limit as $m \to 0$, and so is analytic as a function of m; the limit is $4\pi v_0 a \delta(\omega - \omega_0)$. The strength of the gust, i.e. the spanwise integral of $v_0\, \mathrm{H}(z/a, -1, 1)$, is $2v_0 a$, which is twice the strength of the delta-function and Gaussian gusts analysed in §3.

In expression (3) for the pressure, the integral is not tractable analytically, but from (4) the far-field approximation $p \simeq p_+ + p_-$ is

$$p(x, y, z, t) \simeq \frac{-\rho_0 M c_0 \bar{v}_0 \mathrm{sgn}(y)}{\pi} \mathrm{e}^{-\mathrm{i}\omega_0(t - M\bar{x}/c_0)} \frac{2\bar{a}}{\bar{R}_h} \cos(k\bar{R}_h) \frac{\sin(k\bar{a}\tan\bar{\theta}_h)}{k\bar{a}\tan\bar{\theta}_h}. \tag{36}$$

In the limit $a \to 0$ and $v_0 \to \infty$, with $v_0 a$ fixed, this is twice the field (7) of a delta-function gust with strength $v_0 a$, as expected. Much of the discussion in §3.2 of the far-field of a Gaussian gust applies also to (36). The main difference is that the directivity function, which was $\mathrm{e}^{-(k\bar{a}\tan\bar{\theta}_h)^2/2}$ for the Gaussian gust, is now the final term in (36), i.e. the function $\mathrm{sinc}(s) = \sin(s)/s$ with argument $s = k\bar{a}\tan\bar{\theta}_h$; recall that $\tan\bar{\theta}_h = -\bar{z}/\bar{R}_h$. This directivity function is multi-lobed, with lobes of progressively smaller amplitude as $|\tan\bar{\theta}_h|$ increases. The central lobe occupies a region about the z-plane bounded by $|\tan\bar{\theta}_h| = \pi/(k\bar{a})$, so that at high frequencies this region is narrow, whereas at low frequencies it fills the Mach cone almost completely. As the frequency increases, the the amplitude of the lobes decays more rapidly with increasing $|\tan\bar{\theta}_h|$, so that the entire field, not just the central lobe, becomes confined to a progressively narrower zone about the plane $z = 0$. The sinc-function directivity is well known in diffraction theory, but with an angular argument different from the hyperbolic angle $\bar{\theta}_h$ we are using here.

Figures 6(a, b) give contour plots of the pressure field on vertical transverse sections for Mach number $M = \sqrt{2}$ and Helmholtz number $k\bar{a} = 4$. The sections are at $\bar{x} = \bar{b}/4$ and $\bar{x} = 2\bar{b}$, where $\bar{b} = 4k\bar{a}^2$ is the Rayleigh distance based on wavenumber k and source width $2a$, i.e. the distance at which (provided $2k\bar{a} > 1$) far-field approximations start to apply . Thus plot (a) gives the near field, and plot (b) gives the far field. The plots have been obtained by accurate numerical evaluation of (11) with $g(z)$ in (9) taken to be $\mathrm{H}(z/a, -1, 1)$; for plot (b), the far-field approximation (36) may also be used, as the difference between the exact and approximate formulae rapidly becomes indistinguishable when $\bar{x}$ increases beyond about $4k\bar{a}^2$.

5.1. The Fresnel approximation

The Fresnel approximation to the acoustic field produced by the top-hat gust is of the form $p = (p_+ - p_-)/2$, where $p_\pm$ are obtained from (21) and (22) by replacing z by $z \pm a$, and $\bar{R}_h$ by $\bar{R}_{h\pm}$, as defined in (34). Just as for the anti-symmetric and Heaviside gusts, the only region in which the Fresnel approximation loses accuracy is close to the leading edge, i.e. for $k\bar{r}_h \lesssim 1$. In Figures 6(a, b), the approximate fields would be indistinguishable from the exact fields plotted. In order to see a difference between exact and approximate fields, it would be necessary to take a section at a value of x such that $k\bar{x} \lesssim 1$.

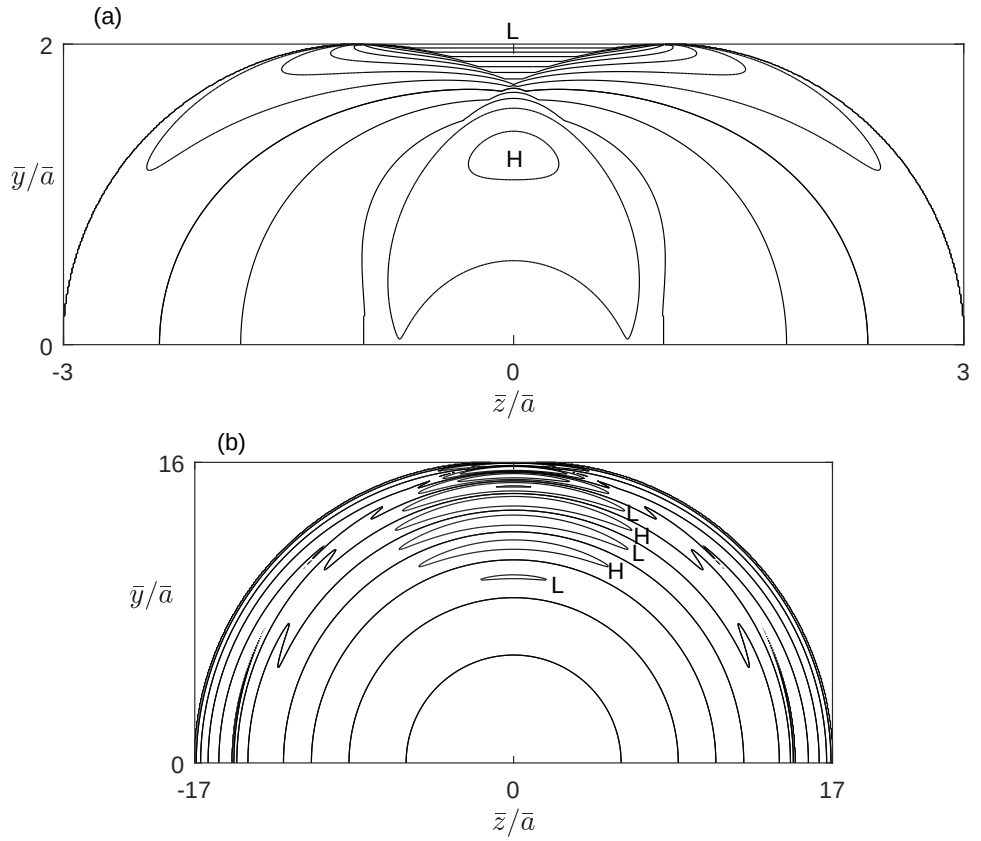

Figure 6: Scaled pressure contours for the top-hat gust on vertical sections (a) $\bar{x} = \bar{b}/4$ and (b) $\bar{x} = 2\bar{b}$ for Mach number $M = \sqrt{2}$ and Helmholtz number $k\bar{a} = 4$; the Rayleigh distance $\bar{b} = 4k\bar{a}^2$ is based on free-space wavenumber k and source width $2a$. Contour values in (a) are -1.0 to 0.4, and in (b) are $-.05$ to 0.05, marked low (L) to high (H). The Mach cones from the edges $z = \pm a$ of the gust are dominant features in (a), but can only just be seen in (b).

5.2. The Keller approximation

A ray theory approximation to the pressure field may be obtained by applying the method of §4.1.2 to the functions $p_\pm$ just defined for the Fresnel approximation. This gives coefficients $(\alpha_\pm, \beta_\pm, \gamma_\pm)$ obtained from (26) on replacing z by $z \pm a$, and $\bar{R}_h$ by $\bar{R}_{h\pm}$. The resulting approximation to $(p_+ - p_-)/2$ is

$$p(x,y,z,t) \simeq \frac{-\rho_0 M c_0 \bar{v}_0 \,\mathrm{sgn}(y)}{\pi} \mathrm{e}^{-\mathrm{i}\omega_0(t-M\bar{x}/c_0)} \left\{ \frac{\sin(k\bar{R}_{h-})}{k(\bar{z}-\bar{a})} - \frac{\sin(k\bar{R}_{h+})}{k(\bar{z}+\bar{a})} + (2\pi)^{1/2} H\left(\frac{z}{a}, -1, 1\right) \frac{\cos(k\bar{r}_h - \pi/4)}{(k\bar{r}_h)^{1/2}} \right\}. \quad (37)$$

Because of the singular surfaces $z = \pm a$, this approximation applies outside of two surfaces of the form (28), with z replaced by $z \pm a$. In Figures 6(a, b), this would correspond to the region outside of the two oval shaped curves obtained as translations of the oval curves in Figures 5(a, b) by $\pm k\bar{a}$ in the z direction.

Expression (37) may be simplified when $|z| \gg a$. In this case, the two-dimensional term in $\mathrm{H}(z/a, -1, 1)$ is no longer present, the terms $\bar{z} \pm \bar{a}$ in the denominators may be replaced by $\bar{z}$, and the terms $\bar{R}_{h\pm}$ may be replaced by their binomial approximations

$$\bar{R}_{h\pm} \simeq \bar{R}_h \left(1 \mp \frac{\bar{a}\bar{z}}{\bar{R}_h^2}\right) = \bar{R}_h \pm \bar{a} \tan\bar{\theta}_h. \quad (38)$$

After simplification, the result is the far-field approximation (36). At first sight this is unexpected, because the starting point here is equation (37), which does not apply near the singular surfaces $z = \pm a$, but the end result, equation (36),

suffers no such restriction, and is in fact perfectly smooth and uniform in z. The explanation is that in passing from (37) to (36) the singularities arising from terms in $\pm a$ have cancelled out, in effect by being placed on the same surface, namely $z = 0$; and of course the singularities are not present either in the exact solution or in the uniform approximation based on the Fresnel integrals (22). One should emphasize, nevertheless, the usefulness of approximation (37), because of its simplicity and the fact that it applies in such a large region. It is a ray theory representation of the sound field, accounting both for the spherically spreading rays from the points $z = \pm a$ and the cylindrically spreading rays from the leading edge, in accord with Keller's geometrical theory of diffraction.

The mathematical details justifying the above remarks are presented in [18]. The analysis depends on the two surfaces of the form (28) with z replaced by $z \pm a$, these being approximation boundaries for $p_{\pm}$. The region inside both surfaces begins at a value of $\bar{r}_h$ given by

$$\frac{\bar{r}_h}{\bar{a}} = \frac{4}{\pi\sigma^2} k\bar{a} + \frac{\pi\sigma^2}{16} \frac{1}{k\bar{a}}, \tag{39}$$

and beyond this value of $\bar{r}_h$ the far-field approximation (36) applies. For $k\bar{a} > 1$, equation (39) is in order of magnitude $\bar{r}_h/\bar{a} = 4k\bar{a}$ when $\sigma = 0.5$, so that $\bar{r}_h$ is then the Rayleigh distance $4k\bar{a}^2$, beyond which the far field begins.

6. Conclusion

In this paper, the authors have derived in a uniform way the main three-dimensional canonical sound fields produced by a single-frequency gust striking the leading edge of a flat plate at zero angle of attack in a supersonic mean flow. These canonical sound fields are an idealization of the sound fields which arise in practice, for example as produced by aeroengine fan blades. But they have the merit of making explicit the sound fields which occur in important reference flows, including their complete parametric dependence, and they provide a way of understanding the complexities of more realistic studies.

Mathematically, the most striking feature of the results is their analogy to many classical results of diffraction theory, involving sound (or light) striking a screen or aperture. Two transformations are needed: first to Doppler-adjusted Cartesian coordinates, as defined by Eqn (1), and second to hyperbolic polar coordinates, as defined after Eqns (3) and (4). In these coordinates, many of the equations are formally related to known equations; moreover, certain key concepts, such as the Rayleigh distance and Fraunhofer diffraction pattern, have immediate analogues in the transformed variables. Although the Mach cone is unique to supersonic flow, we have seen that many high-frequency fields are effectively localised to a small region within it, especially the Fresnel diffraction region adjacent to a shadow boundary; in this situation, the main field is not strongly influenced by the Mach cone. Most interesting of all, we have found sound fields with a ray structure that can immediately be interpreted in terms of Keller's geometrical theory of diffraction, but expressed in hyperbolic coordinates. This is extremely promising for development of the transonic and supersonic branches of the subject as part of diffraction theory.

References

[1] M. R. Myers, E. J. Kerschen, Influence of camber on sound generation by airfoils interacting with high-frequency gusts, J. Fluid Mech. 353 (1997) 221–259.

[2] L. J. Ayton, An analytic solution for gust-aerofoil interaction noise including effects of geometry, IMA Journal of Applied Mathematics 82 (2017) 280–304. doi:10.1093/imamat/hxw038

[3] R. K. Amiet, Acoustic radiation from an airfoil in a turbulent stream. J. Sound Vib. 41 (1975) 407-420.

[4] S. J. Majumdar, N. Peake, Three-dimensional effects in cascade-gust interaction, Wave Motion 23 (1996) 321-337.

[5] Y. P. Guo, A note on sound from the interruption of a cylindrical flow by a semi-infinite aerofoil of subsonic speed, J. Sound Vib. 128 (1989) 275–286.

[6] C.J. Chapman, High-speed leading-edge noise, Proc. Roy. Soc. A 459 (2003) 2131–2151.

[7] C.J. Chapman, Some benchmark problems for computational aeroacoustics, J. Sound Vib. 270 (2004) 495–508.

[8] C. J. Chapman, Sesquipoles in aeroacoustics, J. Sound Vib. 300 (2007) 1015-1033.

[9] I. Evers, N. Peake, Noise generation by high-frequency gusts interacting with an airfoil in transonic flow, J. Fluid Mech. 411 (2000) 91–130.

[10] C. J. Powles, Noise generation by a supersonic leading edge. Part 2: examples of two-dimensional sound fields, J. Sound Vib. 276 (2004) 853–868.

[11] S. Zhong, X. Zhang, J. Gill, R. Fattah, Y. Sun, A numerical investigation of the sound produced by airfoil-gust and shock-gust interaction in transonic flow, J. Sound Vib. (2018) (in press).

[12] J. E. Ffowcs Williams, Y. P. Guo, Sound generated from the interruption of a steady flow by a supersonically moving aerofoil, J. Fluid Mech. 195 (1988) 113–135.
[13] Y. P. Guo, On sound generation by a jet flow passing a semi-infinite aerofoil, AIAA paper 89-1070, Reston, VA: American Institute of Aeronautics and Astronautics (1989) 1–10.
[14] Y. P. Guo, Sound generation by a supersonic aerofoil cutting through a steady jet flow, J. Fluid Mech. 216 (1990) 193–212.
[15] N. Peake, Unsteady transonic flow past a quarter-plane, J. Fluid Mech. 244 (1992) 377-404.
[16] N. Peake, The interaction between a steady jet flow and a supersonic blade tip, J. Fluid Mech. 248 (1993) 543–566.
[17] N. Peake, The scattering of vorticity waves by a supersonic rectangular wing, Wave Motion 25 (1997) 369–383.
[18] C. J. Powles, Supersonic leading-edge noise, PhD thesis, University of Keele (2004).
[19] C. J. Powles, Noise generation by a supersonic leading edge. Part 1. General theory, J. Sound Vib. 276 (2004) 837–852.
[20] C. J. Chapman, C. J. Powles, Basic singular fields in the theory of impulsive supersonic leading-edge noise, Wave Motion (2019) (in preparation).
[21] N. Peake, A. B. Parry, Modern challenges facing turbomachinery aeroacoustics, Annual Review of Fluid Mechanics 44 (2012) 227–248.
[22] L.B. Felsen and N. Marcuvitz, *Radiation and Scattering of Waves*, Institute of Electrical and Electronic Engineers Press, New York, 1994.